Title
LQG Dynamic Positioning for a Supply Vessel

Permalink
https://escholarship.org/uc/item/8bg22820

Author
Hansen, Scott Ron

Publication Date
2013

Peer reviewed|Thesis/dissertation

UNIVERSITY OF CALIFORNIA, SAN DIEGO

LQG Dynamic Positioning for a Supply Vessel

A Thesis submitted in partial satisfaction of the
requirements for the degree Master of Science

in

Engineering Sciences (Aerospace Engineering)

by

Scott Ron Hansen

Committee in charge:

Professor Mauricio de Oliveira, Chair
Professor Juan Carlos del Alamo
Professor Thomas Bewley

2013

The Thesis of Scott Ron Hansen is approved, and it is acceptable in quality

and form for publication on microfilm and electronically:

Chair

University of California, San Diego

2013

TABLE OF CONTENTS

LIST OF ABBREVIATIONS

DP	Dynamic Positioning
AUV	Autonomous Underwater Vehicle
IMO	International Maritime Organization
CG	Center of Gravity
CB	Center of Buoyancy
GPS	Global Positioning System
DGPS	Differential Global Positioning System
LTW	Light Taut Wire
DARPS	Differential, Absolute and Relative Positioning System
CFD	Computational Fluid Dynamics
MSS	Marine Systems Simulator
NED	North-East-Down
LQG	Linear Quadratic Gaussian
LQR	Linear Quadratic Regulator
LQE	Linear Quadratic Estimator
LTI	Linear Time-Invariant
LTV	Linear Time-Varying
LHP	Left Hand Plane
PID	Proportional Integral Differential

LIST OF FIGURES

LIST OF TABLES

ACKNOWLEDGEMENTS

I would like to acknowledge a few individuals who were instrumental in this thesis starting with Professor Mauricio de Oliveira. I am thankful that he allowed me to pursue an interest of mine but I will always be grateful for the continual assistance he provided me during this evolution. I can honestly say that he went above and beyond to provide not just guidance but the critical clarification when I was so confused that the only word I could conjure up was "What?". Tackling a project like this without having a mechanical background was a difficult task which would have simply been impossible without the clarity and patience I received from Mauricio de Oliveira on a regular basis. I can't thank him enough for the countless hours of assistance. That being said, I also want to thank his wife for the time he has spent late on campus clearing up the muddy waters that resided in my head. I say this because I was sitting with him late one night and when we finished Mauricio de Oliveira made a comment that he should get home since it was their anniversary and all I could think was why he didn't just tell me he couldn't meet up.

I should also thank John Thornton for giving me the push to go back to college and get my Masters. I had always thought about going back but I guess I just got comfortable and kept thinking that I would get around to it one day. I can honestly say that if it wasn't for that push I would still be "getting around to it".

Lastly, I would like to acknowledge my fiancée Christine Busa for all her support and aid throughout this process. I know everyone thanks their significant other in these papers but I really have to acknowledge the woman who did literally everything for me while I was pursuing this degree. She made the entire task significantly easier and took a ton of weight off my back. She put up with all the sleepless nights, lack of together time, and the negative vibes I radiated on a regular basis. I know it couldn't have been easy and I am forever thankful that

I have such a strong woman by my side. I've spent the past year unable to aid her in the wedding plans and her taking it all in stride. Now I can get back to focusing on the most important thing in my life … my future wife. Love you Sweets.

ABSTRACT OF THE THESIS

LQG Dynamic Positioning for a Supply Vessel

by

Scott Ron Hansen

Master of Science in Engineering Sciences (Aerospace Engineering)

University of California, San Diego, 2013

Professor Mauricio de Oliveira, Chair

The purpose of this study is to merge my on the job marine experience and the control knowledge gathered throughout my studies at University of California San Diego into a practical control design.

This thesis creates a Dynamic Positioning (DP) control loop for a supply vessel which utilizes two azimuthal thrusters as actuators. The control loop is designed to also account for external environmental disturbances and sensor measurement noise. The control loop is accomplished using modern control theory which makes use of known vessel dynamics and assumptions associated with the environment and sensor measurement variances.

During this thesis research and design period, a testing platform for the control loop was required. Without the ability to retrofit a physical vessel with the proposed azimuthal thrusters it was determined that a simulation model would be required and was designed and implemented in Matlab Simulink to allow for control loop testing and validation. This simulation model is presented as part of the thesis research and design flow as it was a required element of the design and encompasses the knowledge acquired in my marine work and during my period at UCSD.

Control loop performance results were obtained through testing on the generated simulation model. These results allowed for validation and optimization during the design phases of the vessel control loop.

The principal conclusions were that the simulation model provided sufficient dynamics to properly execute the required tests to the control loop and that the implemented control loop was capable of operating within the determined parameters set forth in the design validation testing.

Chapter 1

Introduction

1.1. Dynamic Positioning

Dynamic Positioning (DP) in its simplest form is a system used for maintaining a desired position over a point on the ocean floor regardless of outside environmental disturbances. According to the Norwegian classification society DnV (1990) a DP vessel is defined as [1]:

Dynamically positioned vessel: a free-floating vessel which maintains its position (fixed or predetermined track) exclusively by means of thrusters.

DP systems typically account for positional control in the XY plane where rotation (yaw or heading) may or may not be a requirement. Extension from the 3 DOF (x, y, ψ) to 5 DOF $(x, y, \phi, \theta, \psi)$ which incorporates pitch and roll dampening has become more useful with semi-submersible vessels in recent years [2]. The ability to hold position becomes most relevant in situations which may limit or prevent the use of anchors. Vessels which routinely

utilize DP control loops include oil rigs, research vessels, supply ships, and Autonomous Underwater Vehicles (AUVs). These vessels rely on DP to compensate for environmental disturbances which are difficult for an operator to properly account for in real time. Vessels in the deepest areas of the ocean can be affected by excessive winds and waves where a well-designed DP controller can anticipate these changes and compensate for them such that the vessel remains within the desired scope for the mission. Winds and waves frequently change in both amplitude and direction while ocean current is reasonably consistent when a vessel is not within littoral (near shore) waters. There are a wide range of sensors which can be found on vessels that can determine these disturbances accurately. These sensors are utilized by main ship control and the DP system however, it is important to note that most DP schemes are independent from main shipboard control which consists of the main propulsion and rudders. This independence is due to the supporting nature of the DP controller which can be used in not just holding of position but also slowly transitioning to another location (marked positioning) [1].

1.1.1. Classes of Dynamic Positioning Systems

Based on International Maritime Organization (IMO) publication [3] the Classification Societies have issued rules for Dynamic Positioning Ships described as Class 1, Class 2, and Class 3 which relate to equipment failures.

- Equipment Class 1 has no redundancy.
  - Loss of position may occur in the event of a single fault.
- Equipment Class 2 has redundancy so that no single fault in an active system will cause the system to fail.
  - Loss of position should not occur from a single fault of an active component or system such as generators, thruster, switchboards,

remote controlled valves etc., but may occur after failure of a static component such as cables, pipes, manual valves etc.

- Equipment Class 3 which also has to withstand fire or flood in any one compartment without the system failing.

  o Loss of position should not occur from any single failure including completely burnt fire sub division or flooded watertight compartment.

1.1.2.   Sensors

Over the years there have been several approaches to determine a ships position accurately enough to perform DP. Generally, the Global Positioning System (GPS) isn't accurate enough to perform DP so additions to the system have been incorporated to increase accuracy. One such system is using Differential GPS (DGPS) which uses a transmission from a fixed ground-based reference station and then compares the GPS reading on the ship with the known ground location to determine the actual position. A similar approach to the DGPS uses a transponder installed at a fixed reference point on the ocean floor. The transponder communicates acoustically from the ship to acquire reference data to calculate position [3]. These two systems are similar to each other since they use a reference point to perform a differential calculation of the ship's position. There are also mechanical means to gain positional information by measuring the riser angle deflections on drill ships to perform DP. Another mechanical system is a light taut wire (LTW) method which was used frequently in the past. LTW method used a clump weight lowered to the ocean floor and the system measured the length of cable paid out along with the angle to calculate the vessel's position [3]. The problem with these last two methods is that they can only be done in fairly shallow water since they require connection to the ocean floor. In deep ocean applications, the DGPS is an easier DP system to implement and maintain. There are a few other position acquisition

systems such as: Fanbeam and CyScan, Artemis, Differential Absolute and Relative Positioning System (DARPS), RADius and RadaScan, and inertial navigation units [3].

The discussion above presents a multitude of options when it comes to determining the (x,y) position in the XY plane but when it comes to determining the heading (yaw) of an ocean vessel it is normally done using a gyrocompass. There are several types of gyrocompasses such as the Ring-Laser gyroscopes, Fibre optic gyroscopes and Seapat which uses a combination of GPS and inertial sensors [3].

When it comes to environmental sensors there are wind and draught sensors which can also feed into the DP control loop. Wind sensors are used to do a feed forward approach on the controller where the draught sensor would be used to help the control loop understand how much of the vessel is susceptible to wind and current effects [3].

1.1.3.   Actuators

Vessels equipped with a DP scheme have additional actuators outside of the main propulsion. This configuration is necessary since the DP actuators are typically designed for slow speed operation while primary propulsion is generally for navigation over great distances. Most often these additional actuators are in the form of azimuthal and tunnel thrusters.

1.1.3.1. Azimuthal Thrusters

Azimuthal thrusters are propellers which are mounted on the bottom of the vessel and have the ability to generate vectored thrust in the XY plane. This system has one or more propellers which can be trained such that the operator is capable of getting the desired thrust level in the direction best suited for the situation. Azimuthal thrusters are effective propulsion units for DP systems due to their unlimited variability and resolution in both direction and

amplitude of thrust. The variability can also create issues in the control loop design since they provide a multitude of solutions to the same problem.

There are several types of azimuthal thrusters classically employed on DP vessels: single propeller, counter-rotating propeller and pump jet designs. The single and counter-rotating propeller systems have propellers hanging below the vessel in the flow stream. These are the most efficient systems and most widely used however, they frequently have operational speed limitations. These limitations are the result of them hanging in the flow stream and due to the hydrodynamic loading at higher velocities. If a vessel requires higher speed these azimuthal thrusters are sometimes retractable into the vessel's hull. Pump jet azimuthal thrusters are mounted flush with the hull of the vessel and operate by pumping ocean water up into the pump jet and redirected out through a trainable nozzle. This nozzle has some losses in the output thrust since the vectored thrust will have a small z-axis component. The pump jet also has losses in the cross flow over the inlet. This makes the azimuthal thruster less efficient than its previously mentioned counter-part but has an advantage at higher speeds. Since the pump jet is mounted flush with the bottom of the vessel there is no hydrodynamic loading and is able to operate at speeds without fear of damage.

1.1.3.2. Tunnel Thrusters

Tunnel thrusters are sometimes referred to as bow thrusters since the early implementations were put into the bow to aid in turning the vessels which were either very large or operated at slow speeds. This would subsequently restrict the effectiveness of the rudder. Today stern mounted tunnel thrusters can add significant control to a DP control loop as well. Tunnel thrusters are permanently mounted in a vessel with a cylinder which runs through the hull of a vessel and connects the port and starboard waters. A propeller is mounted internal to the cylinder and pumps ocean water from one side to the other. These

thrusters are only capable of providing a y-axis force and yaw moment dependent on the distance from CG (center of gravity). Because of this limitation with respect to providing force in the x-axis a tunnel thruster is frequently used in conjunction with an azimuthal thruster.

1.2. Scope of Thesis

Given the background information detailed above, the approach in this thesis was to create a 3 DOF (x, y, ψ) DP controller with specified sensor inputs, actuator controls, vessel, and environmental effects. The sensors selected for this DP controller are a GPS for the position data and a gyrocompass for the vessel's heading. Due to the lack of an actual test platform the vessel had to be simulated and therefore, the sensor data also required simulation. White noise was applied to both sensor inputs to the control loop to properly simulate sensor noise which could be present in a real application. The simulated vessel is only using one sensor input for acquisition of the position and heading data therefore this system is by definition an Equipment Class 1 DP controller due to the lack of any redundancy. Since this is a simulation, there is no necessity to design the controller as an Equipment Class 2 DP since there is no fear of sensor failure. The vessel parameters selected for simulation and DP control were based on a Viking Energy supply vessel as shown in Figure 1. This particular vessel was selected due to the Computational Fluid Dynamics (CFD) data available from Thor Fossen and Tristan Perez's Marine Systems Simulator (MSS) download page [4]. This vessel is outfitted with two azimuthal thrusters (one forward and one aft) on the centerline of the vessel. Tunnel thrusters were not used in this thesis since that is a typical convention and an aft azimuthal thruster is not frequently accompanied with a forward azimuthal thruster. Using

this approach adds capability and complexity which will be discussed in the following sections.

Environmental disturbances that were selected for this simulation were ocean current, wind and waves. The ocean current is a constant current in a specified direction where the wind and waves are varying in direction and magnitude.

This thesis is broken into three phases: Introduction, Simulation, and Controller Design and Evaluation. This completes the introduction portion of this paper. In the simulation section, the non-linear equations of motion of the vessel are implemented to simulate, as accurately as possible, the actual supply ship responding to forces applied from the environment and thrusters. The controller section is the linearized controller which is applied to the Viking vessel to hold position. The testing section will detail the results of this approach and the capabilities and deficiencies of the DP system. The controller design and testing are grouped together since the nature of the implementation required a repetitive approach that involved several design and test iterations.

Figure 1: Viking Energy Supply Vessel [5]

Chapter 2

Simulation

2.1. Vessel Model

Due to the financial limitations a test platform was unavailable for implementation and testing of the DP controller. Instead, a test bed was designed to replicate the behavior of the selected vessel. This test bed was designed using non-linear equations of motion for the vessel. There are a few vessel simulation software components available which could have been modified for use in this thesis however, as a Computer Engineer by trade the exercise of building a mechanical representation of the final platform was valuable in the understanding of this DP controller implementation.

In designing the simulation, since this is a DP controller for a surface ship operating within the XY plane, the approach was to design the controller and simulation as a 3 DOF system. The vector representation of the positions/Euler angle, velocities and external forces/moment are defined in Equation 1. It is important to note that for consistency purposes most variable definition convention is based on Thor I. Fossen's "Handbook of Marine Craft Hydrodynamics and Motion Control" which was a primary reference for this project.

$$\boldsymbol{\eta} = [x \quad y \quad \psi]^T$$

$$\boldsymbol{v} = [u \quad v \quad r]^T$$

$$\boldsymbol{\tau} = [X \quad Y \quad N]^T$$

Equation 1: 3 DOF Defined Position, Velocity, and Force/Moment

2.1.1.   Axis Transformation

When referencing the forward motion of a ship along its X axis it is referred to as *surge* while lateral movement along the Y axis is commonly referred to as *sway* and as mentioned earlier the rotation in the XY plane is denoted as *yaw*. An important item to note is that for marine navigation the geographic reference frame is the North-East-Down (NED) coordinate system which differs from its aviation counterpart. The NED coordinate system is oriented such that the X axis points (positive direction) towards true north, positive Y axis points east and finally the Z axis points downwards normal to the Earth's surface. When discussing the inertial frame it will be referenced as $\{n\} = (x_n, y_n, z_n)$ with $\{n\}$ being the position of the vessel in the inertial frame. When referring to the vessel's body fixed frame it will be referenced as $\{b\} = (x_b, y_b, z_b)$. The fixed point of $\{b\}$ on the vessel can be any point the user desires but the most common locations are the bow, ship center, and CG. There are inherent advantages to placing the origin of the body frame at CG since doing so requires no offset in (x, y, z) from $\{b\}$ to CG. Since the equations of motion used throughout this study are based on the Newton-Euler formulation which relates Newton's second law with respect to the vessel's CG, the origin was placed at CG for this analysis. Figure 2 illustrates the fixed body frame along with labels showing surge, sway, heave, roll, pitch, and yaw.
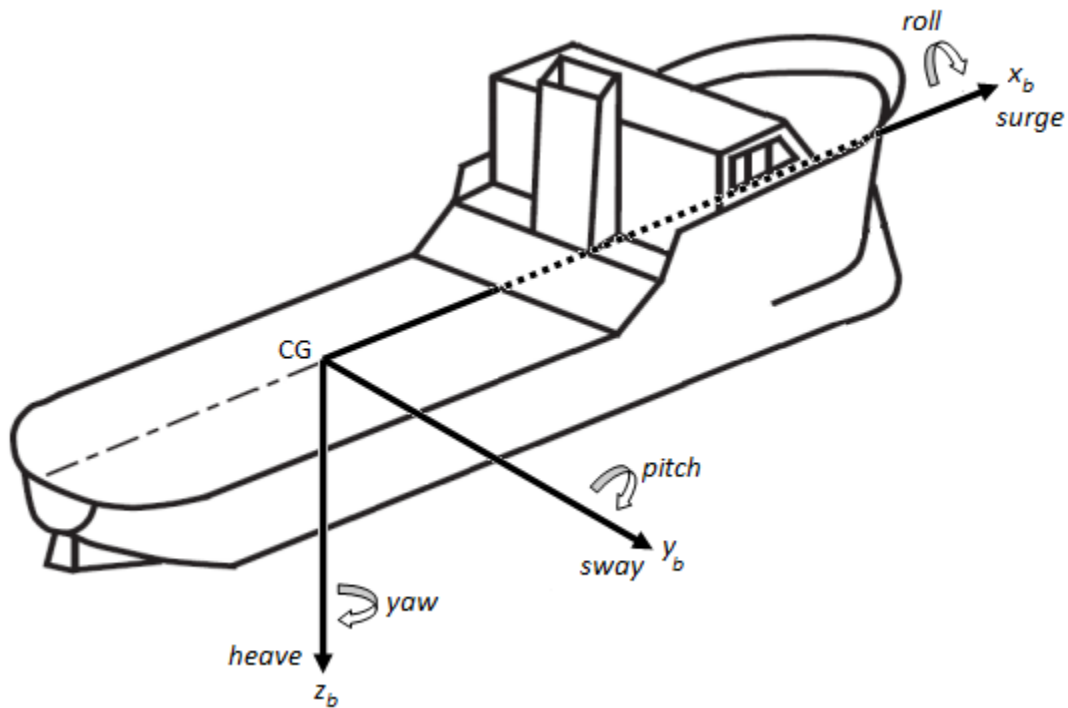
Figure 2: Motion in 6 DOF

When creating the simulation an axis transformation is required to go between the inertial and fixed-body frames. This is necessary since a unit of motion of a vessel in (x,y) (surge and sway) with respect to the fixed-body frame does not translate to a unit in (x,y) respectively in the inertial frame when $\psi \neq 0$. For example, if a ship is facing due east and has a positive velocity in only the surge direction with respect to the fixed-body frame it would equate to a positive translation on the y-axis of the inertial frame. Since the yaw position is a measurement with respect to the inertial frame this provides the means to determine the inertial (x,y) movement from a fixed-body movement. Equation 2 shows how this axis transformation is accomplished using the fixed-body velocity (v_b) to calculate inertial velocity (v_n).

$$v_n = R(\psi)v_b$$

Where:

$$R(\psi) = \begin{bmatrix} cos(\psi) & -sin(\psi) & 0 \\ sin(\psi) & cos(\psi) & 0 \\ 0 & 0 & 1 \end{bmatrix}$$

Equation 2: 3 DOF Axis Transformation

2.1.2.   3 DOF Marine Vessel Equations of Motion

The equations of motion which form the dynamical model of the vessel are shown in vectorial form in Equation 3 and consist of inertia, Coriolis, damping, drag, and restoring forces. It is often the convention to write all equations of motion out into their parametric form and then form the appropriate matrices and vectors to put into vectorial form but in this document it will presented in vectorial form first and then each matrix/vector combination will be discussed individually.

$$v_n = R(\psi)v_b$$

$$M\dot{v} + C(v)v + Dv + d(v_r) + g(\eta) = \tau + \tau_{wind} + \tau_{wave} + \tau_{current}$$

Equation 3: Marine Vessel Equations of Motion (Vectorial Form)

2.1.2.1. Marine Vessel Inertia Matrix

A marine vessel's inertia matrix is a sum of the rigid body and the added mass terms of the vessel. The rigid body is an assumption that the vessel is incompressible and therefore any two points within the vessel will remain at a constant distance from each other regardless of forces or torques applied. The added mass term refers to inertia being added to a system when it is accelerated (or decelerated) through a fluid body. This inertia added to the system is from the displacement of a volume of water which is a result of the inability of both the vessel and the fluid to occupy the same area at the same time. The inertia equations for a

marine vessel are based on Newton's second law of motion (F = ma) and are broken down for

the rigid-body terms in Equation 4.

$$X_{RB} = m(\dot{u} - y_g\dot{r})$$

$$Y_{RB} = m(\dot{v} + x_g\dot{r})$$

$$N_{RB} = I_z\dot{r} + m(x_g\dot{v} - y_g\dot{u})$$

Where:

$$CG = (x_g, y_g, z_g)$$

$$I_z = Inertia\ Tensor$$

Equation 4: Rigid-body Inertia w.r.t. CG

When looking at (x_g, y_g, z_g), it is the distance from the origin of the vessel to the CG

of the vessel. In the case of this design the origin was placed at the CG of the ship which

reduces the equations of motion. From this point on in this documentation the equations will

be simplified according to: $(x_g, y_g, z_g) = (0,0,0)$ as shown in Equation 5.

$$X_{RB} = m\dot{u}$$

$$Y_{RB} = m\dot{v}$$

$$N_{RB} = I_z\dot{r}$$

Equation 5: Rigid-body Inertia

This gives the rigid-body inertia equations for the vessel model to be used in the

simulation. To complete the equations for the inertia matrix the added mass inertia equations

are shown in Equation 6.

$$X_A = -(X_{\dot{u}}\dot{u} + X_{\dot{v}}\dot{v} + X_{\dot{r}}\dot{r})$$

$$Y_A = -(Y_{\dot{u}}\dot{u} + Y_{\dot{v}}\dot{v} + Y_{\dot{r}}\dot{r})$$

$$N_A = -(N_{\dot{u}}\dot{u} + N_{\dot{v}}\dot{v} + N_{\dot{r}}\dot{r})$$

Equation 6: Added Mass Inertia

It is common for surface vessels to decouple the surge mode from the steering dynamics due to XY symmetry [6]. By applying this symmetry relationship, the added mass equations can be further simplified to Equation 7.

$$X_A = -(X_{\dot{u}}\dot{u})$$

$$Y_A = -(Y_{\dot{v}}\dot{v} + Y_{\dot{r}}\dot{r})$$

$$N_A = -(Y_{\dot{r}}\dot{v} + N_{\dot{r}}\dot{r})$$

Equation 7: Simplified Added Mass Inertia

The added mass coefficients $(Y_{\dot{v}}, Y_{\dot{r}}, N_{\dot{r}})$ can be approximated using strip theory of a slender body however, one cannot solve for the surge $(X_{\dot{u}})$ coefficient using 2D strip theory (only 3D programs calculate surge coefficients) [7]. Access to these 3D programs for calculating the surge coefficients were not available during this design phase. In the absence of this tool, the coefficient was approximated at 10% of the vessel's mass. This was suggested as a reasonable approach in discussions with Thor Fossen during the design evolution. This surge coefficient approximation and the calculated slender body strip theory for the remaining coefficients are shown in Equation 8.

$$X_{\dot{u}} = \frac{m}{10} \ (approximation)$$

$$Y_{\dot{v}} = \int_{x_a}^{x_f} \rho \pi r^2 \, dx$$

$$Y_{\dot{r}} = -\int_{x_a}^{x_f} \rho \pi r^2 x \, dx$$

$$N_{\dot{r}} = \int_{x_a}^{x_f} \rho \pi r^2 x^2 \, dx$$

$$N_{\dot{v}} = Y_{\dot{r}}$$

Where:

$$\rho = density \ of \ seawater$$

$$x_f = distance \ from \ CG \ to \ bow$$

$$x_a = distance \ from \ CG \ to \ stern$$

Equation 8: Added Mass Coefficients

Combining the rigid-body and added mass inertia equations and putting into matrix multiplication results in Equation 9.

$$X = m\dot{u} + X_{\dot{u}}\dot{u}$$

$$Y = m\dot{v} + (Y_{\dot{v}}\dot{v} + Y_{\dot{r}}\dot{r})$$

$$N = I_z\dot{r} + (Y_{\dot{r}}\dot{v} + N_{\dot{r}}\dot{r})$$

Matrix Form:

$$\mathbf{M}_{RB} = \begin{bmatrix} m & 0 & 0 \\ 0 & m & 0 \\ 0 & 0 & I_z \end{bmatrix}$$

$$\mathbf{M}_A = -\begin{bmatrix} X_{\dot{u}} & 0 & 0 \\ 0 & Y_{\dot{v}} & Y_{\dot{r}} \\ 0 & Y_{\dot{r}} & N_{\dot{r}} \end{bmatrix}$$

$$\mathbf{M} = \mathbf{M}_{RB} + \mathbf{M}_A$$

$$\boldsymbol{\tau} = \mathbf{M}\dot{\boldsymbol{v}}$$
Equation 9: Inertia Matrix

2.1.2.2. Marine Vessel Coriolis Matrix

The Coriolis matrix also consists of both rigid-body and added mass terms. Newton's laws of motion govern the motion of an object in an (non-accelerating) inertial frame of reference. When Newton's laws are transformed to a uniformly rotating frame of reference (such as the Earth), the Coriolis and centrifugal terms appear [8]. The Coriolis terms are vessel velocity dependent and the rigid-body and added mass terms are detailed in component form in Equation 10 and Equation 11 respectfully. The added mass inertia coefficients $(X_{\dot{u}}, Y_{\dot{v}}, Y_{\dot{r}})$ are used to calculate the Coriolis added mass terms. Again, putting the component form Coriolis equations into vectorial form results in Equation 12.

$$X_{RB}(\boldsymbol{v}) = -muv$$

$$Y_{RB}(\boldsymbol{v}) = muv$$

$$N_{RB}(\boldsymbol{v}) = muv - muv = 0$$

Equation 10: Rigid Body Coriolis

$$X_A(\boldsymbol{v}) = Y_{\dot{v}}v + Y_{\dot{r}}r$$

$$Y_A(\boldsymbol{v}) = -X_{\dot{u}}u$$

$$N_A(\boldsymbol{v}) = X_{\dot{u}}u - Y_{\dot{v}}v - Y_{\dot{r}}r$$

Equation 11: Added Mass Coriolis

$$\boldsymbol{C}_{RB}(\boldsymbol{v}) = \begin{bmatrix} 0 & 0 & -mv \\ 0 & 0 & mu \\ mv & -mu & 0 \end{bmatrix}$$

$$\boldsymbol{C}_A(\boldsymbol{v}) = \begin{bmatrix} 0 & 0 & Y_{\dot{v}}v + Y_{\dot{r}}r \\ 0 & 0 & -X_{\dot{u}}u \\ -Y_{\dot{v}}v - Y_{\dot{r}}r & X_{\dot{u}}u & 0 \end{bmatrix}$$

$$\boldsymbol{C}(\boldsymbol{v}) = \boldsymbol{C}_{RB}(\boldsymbol{v}) + \boldsymbol{C}_A(\boldsymbol{v})$$

$$\boldsymbol{\tau} = \boldsymbol{M}\dot{\boldsymbol{v}} + \boldsymbol{C}(\boldsymbol{v})\boldsymbol{v}$$

Equation 12: Coriolis Matrix

2.1.2.3. Damping Matrix

When looking at the damping forces and moments there are several types to be considered. Potential damping, skin friction, wave drift damping, and damping due to vortex shedding. Most of the damping forces and moments require hydrodynamic software such as WAMIT or ShipX to calculate properly. With the absence of licenses for these applications some damping terms were omitted in the simulation model as discussed in the paragraphs to follow.

Potential damping refers to the radiation-induced damping terms which are often referred to as *linear frequency-dependent potential damping*. This damping term is dependent

on the wave frequency excitation. Skin friction deals with the linear frequency-dependent skin friction due to laminar boundary layer which is experienced at low-frequency motion of a vessel. There is also a high frequency component due to turbulence and is usually referred to as a quadratic or nonlinear skin friction. Wave drift damping is the added resistance for surface ships advancing in waves. Damping due to vortex shedding are forces and moments which are caused by shedding of vortex sheets of a vessel moving through a viscous fluid and is often referred to as *interference drag*. The viscous damping force due to vortex shedding can be modeled using the submerged cross-sectional area of a vessel [6]. For low-speed applications such as DP, damping can be modeled by current coefficients ($C_X, C_Y, \ and \ C_N$) [9]. These coefficients are used to calculate the surge resistance and cross-flow drags. In order to estimate these damping terms the relative current must be calculated to determine the appropriate cross-flow angle of attack. Note that these equations will be presented using relative current terms while the calculation of the angle of attack will be discussed in the ocean current section of the environmental disturbance discussion. The equations of cross-flow drag are contained in Equation 13 and again translated to vectorial form in Equation 14.

$$X_{current} = \frac{1}{2}\rho A_{Fc} C_X(\gamma_{rc}) V_{rc}^2$$

$$Y_{current} = \frac{1}{2}\rho A_{Lc} C_Y(\gamma_{rc}) V_{rc}^2$$

$$N_{current} = \frac{1}{2}\rho A_{Lc} L_{pp} C_N(\gamma_{rc}) V_{rc}^2$$

Where:

$$A_{Fc} = frontal\ cross - sectional\ area$$

$$A_{Lc} = lateral\ cross - sectional\ area$$

$$L_{pp} = length\ between\ perpendiculars$$

$$(C_X, C_Y, C_N) = current\ coefficient\ w.r.t.\ \gamma_{rc}$$

$$\gamma_{rc} = relative\ current\ direction$$

$$V_{rc} = relative\ current\ velocity$$

Equation 13: Cross-Flow Drag

$$\boldsymbol{d}(\boldsymbol{v}_r) = \begin{bmatrix} \frac{1}{2}\rho A_{Fc} C_X(\gamma_{rc}) V_{rc}^2 \\ \frac{1}{2}\rho A_{Lc} C_Y(\gamma_{rc}) V_{rc}^2 \\ \frac{1}{2}\rho A_{Lc} L_{oa} C_N(\gamma_{rc}) V_{rc}^2 \end{bmatrix}$$

Equation 14: Cross-Flow Drag Matrix

In the disturbance section, the relative XY velocity will be discussed and the means of calculation explained. This section, in order to wrap up the non-linear drag, the relative velocity coefficients (C_X, C_Y, C_N) will be discussed in terms of the relative velocity. In practical applications these are typically calculated using CFD software which imports the solid model of the vessel. In this paper, these coefficients were calculated using a sinusoidal approach. This is a reasonable estimation approach for this simulation model with the absence

of these CFD software programs. Equation 15 illustrates the means used to calculate the

coefficients for this model.

$$C_X = -c_{Xmax} * \cos(\gamma_{rc}) * |\cos(\gamma_{rc})|$$

$$C_Y = c_{Ymax} * \sin(\gamma_{rc}) * |\sin(\gamma_{rc})|$$

$$C_N = c_{Nmax} * \sin(2 * \gamma_{rc})$$

Equation 15: Sinusoidal Coefficient

The cross-flow drag components (Equation 14) are quadratic damping (resistance)

terms which will dominate at high speeds but at slow speeds (such as during DP operation) the

linear damping components dominate the system. The linear viscous damping is therefore a

required component to the system model. One means of estimating the linear viscous

damping is illustrated in Equation 16.

$$X_u = -\left(\frac{m + X_{\dot{u}}}{T_{surge}}\right)$$

$$Y_v = -\left(\frac{m + Y_{\dot{v}}}{T_{sway}}\right)$$

$$N_r = -\left(\frac{I_z + N_{\dot{r}}}{T_{yaw}}\right)$$

Where:

$$(T_{surge}, T_{sway}, T_{yaw}) = vessel's\ natural\ frequency\ time\ constants$$

Equation 16: Linear Viscous Damping

$$D = \begin{bmatrix} X_u & 0 & 0 \\ 0 & Y_v & 0 \\ 0 & 0 & N_r \end{bmatrix}$$

Equation 17: Linear Viscous Damping Matrix

Continuing to build the simulation model equations of motion, adding the damping and drag calculations results in Equation 18.

$$\tau = M(\dot{v}) + C(v)v + Dv_r + d(v_r)$$

Equation 18: Equations of Motion

2.1.2.4. Restoring Forces and Moments

The restoring forces and moments for surface vessels are non-existent when looking at 3DOF. This is because $(X_{restore}, Y_{restore}, N_{restore})$ each incorporate pitch or roll terms which are zero which cancel out as shown in Equation 19.

$$X_{restore} = -\rho g \int_0^z A_{wp}(\zeta)d\zeta \sin(\theta) = 0$$

$$Y_{restore} = \rho g \int_0^z A_{wp}(\zeta)d\zeta \cos(\theta)\sin(\phi) = 0$$

$$N_{restore} = pg\nabla\left(-\overline{GM_L}\cos(\theta) + \overline{GM_T}\right)\sin(\phi)\sin(\theta) = 0$$

Where:

$$(\phi, \theta) = (roll, pitch) = (0,0)$$

Equation 19: Restoring Forces and Moment

Removing the restoring forces and moments from the equations of motion results in Equation 20. Figure 3 shows the Simulink implementation of the vessel equations of motion in block form. Since this simulation was strictly done in Simulink instead of in a text based programming language the inclusion of code is difficult. Therefore, code is available upon request and will not be included in this documentation. Given that the equations of motion are defined the only pieces that need to be applied at this point in the simulation are environmental disturbances, expressed in forces and moment $(\tau_{current}, \tau_{wind}, \tau_{waves})$.

$$\boldsymbol{M\dot{v} + C(v)v + Dv + d(v_r) = \tau + \tau_{wind} + \tau_{wave} + \tau_{current}}$$

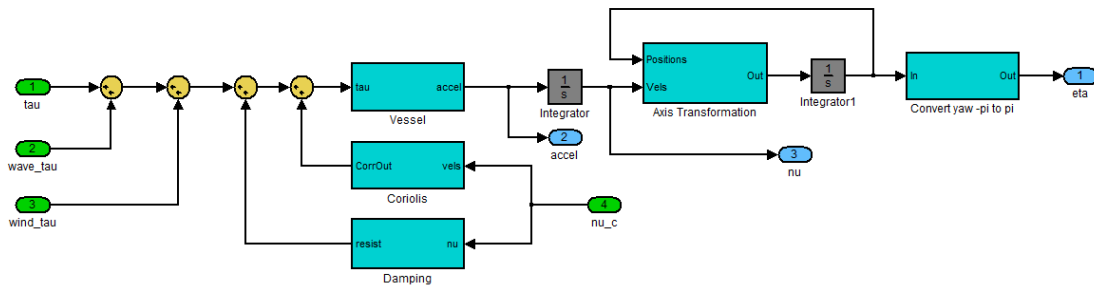Equation 20: Final Equations of Motion

Figure 3: Simulink Equations of Motion

2.2. Disturbances

2.2.1. Ocean Current

Oceanic currents are driven by several factors. One is the rise and fall of the tides, which is driven by the gravitational attraction of the sun and moon on Earth's oceans. Tides create a current in the ocean, near the shore, and in bays and estuaries along the coast. These are called "tidal currents." Tidal currents are the only type of currents that change in a very regular pattern and can be predicted for future dates.

A second factor that drives ocean currents is wind. Winds drive currents that are at or near the ocean's surface. These currents are generally measured in meters per second or in knots (1 knot = 1.15 miles per hour or 1.85 kilometers per hour). Winds drive currents near coastal areas on a localized scale and in the open ocean on a global scale.

A third factor that drives currents is thermohaline circulation - a process driven by density differences in water due to temperature (thermo) and salinity (haline) in different parts

of the ocean. Currents driven by thermohaline circulation occur at both deep and shallow ocean levels and move much slower than tidal or surface currents [10]. Figure 4 gives an overview of global ocean currents. Most global currents are less than 1.0 meter per second however; the Gulf Stream can reach speeds in excess of 1.5 meters per second [12].
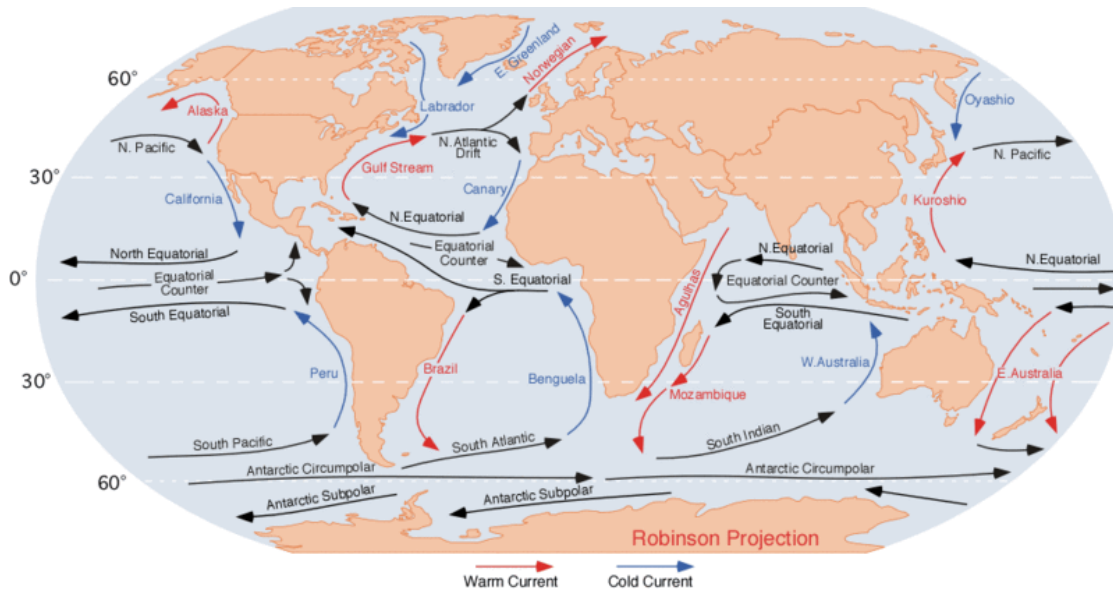

Figure 4: Ocean Currents [11]

When implementing a current environmental disturbance the relative angle to the vessel must be calculated. Determining the angle is done by defining it relative to the bow using a counter-clockwise rotation. Figure 5 illustrates the process for establishing the cross-flow angle of current flow. Equation 21 calculates the angle of attack and magnitude of relative velocity. Using this relative velocity and angle it is now possible to calculate the non-linear drag (Equation 13) correctly which accounts for both the vessel's XY velocity and the current velocity.

$$\gamma_{rc} = \psi - \beta_c - \pi$$

$$V_{rc} = \sqrt{u_{rc}^2 + v_{rc}^2} = \sqrt{(u - u_c)^2 + (v - v_c)^2}$$

Where:

$$\gamma_{rc} = current\ relative\ angle\ of\ attack$$

$$\psi = vessel\ heading$$

$$\beta_c = current\ inertial\ frame\ direction$$
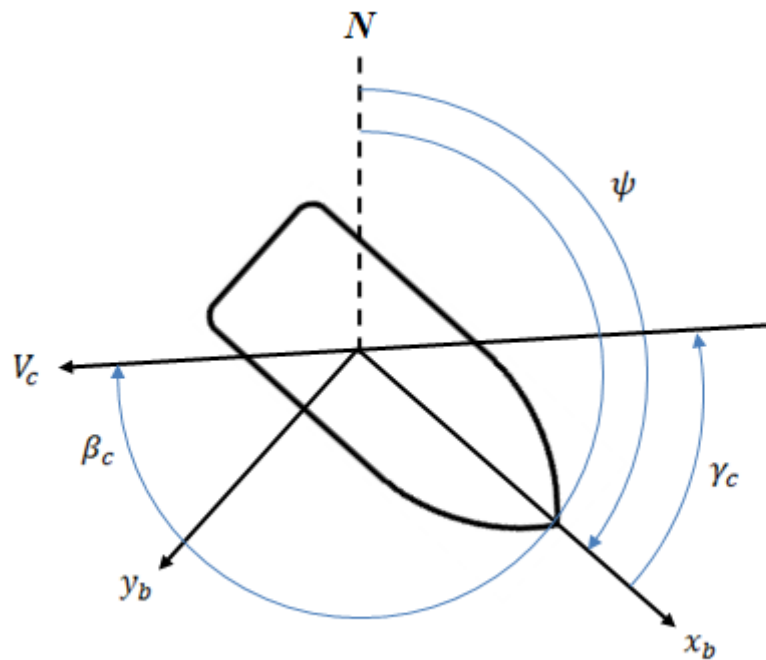
Equation 21: Relative Current Calculation

Figure 5: Current Angle of Attack Relative to Bow [13]

2.2.2.   Waves

In order to properly demonstrate a DP control loop, wave disturbances need to be incorporated in the simulation to evaluate the performance in the presence of waves. When

adding the waves there are two types of induced forces which effect the vessel (first-order and second-order). First-order wave-induced forces are wave-frequency motion observed as zero-mean oscillatory motions. Second-order wave-induced forces are wave drift forces observed as non-zero slowly varying components [14]. The wave disturbance used in this simulation was a Simulink block acquired from the Marine Systems Simulator (MSS) which uses the vessel dataset obtained from the same location [4]. When using the Simulink block it requires Response Amplitude Operators (RAOs) tables to be computed using a hydrodynamic program such as ShipX (2D potential theory) or WAMIT (3D Potential Theory). Since these hydrodynamic programs were not accessible during this evolution it was imperative to utilize the dataset on the supply vessel to get reasonably accurate first and second order wave forces and moments (Equation 22). Figure 6 shows an example of a sea state realization applied to the simulation.

$$\boldsymbol{\tau}_{wave} = \boldsymbol{\tau}_{wave1} + \boldsymbol{\tau}_{wave2}$$

Where:

$$\boldsymbol{\tau}_{wave1} = first\ order\ wave\ induced\ forces\ and\ moments$$

$$\boldsymbol{\tau}_{wave2} = second\ order\ wave\ induced\ forces\ and\ moments$$

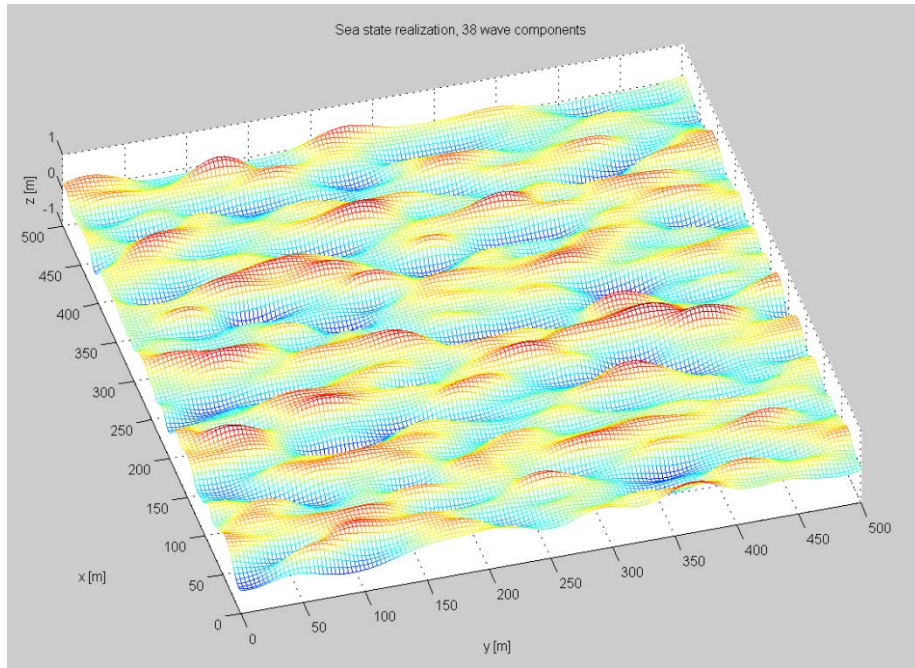Equation 22: Total Wave Forces and Moments

Figure 6: Sea State Realization

2.2.3.   Wind

Wind was added to the simulation model as another environmental disturbance which, unlike the other two environmental inputs, only affects the non-submerged section of the ship. The vessel dataset selected for this simulation does not contain information about the non-submerged sections of the vessel so certain estimations were required in order to get a reasonable model of the ship's responses to the wind forces. The wind model calculations for forces and relative angle of attack applied to the system are similar to the formulas for current (Equation 23 thru Equation 25).

$$X_{wind} = \frac{1}{2}\rho_w V_{rw}^2 C_{Xw}(\gamma_{rw})A_{Fw}$$

$$Y_{wind} = \frac{1}{2}\rho_w V_{rw}^2 C_{Yw}(\gamma_{rw})A_{Lw}$$

$$N_{wind} = \frac{1}{2}\rho_w V_{rw}^2 C_{Nw}(\gamma_{rw})A_{Lw}L_{oa}$$

Where:

$$\rho_w = air\ density$$

$$A_{Fw} = unsubmerged\ frontal\ cross-sectional\ area$$

$$A_{Lw} = unsubmerged\ lateral\ cross-sectional\ area$$

$$L_{oa} = overall\ vessel\ length$$

$$(C_{Xw}, C_{Yw}, C_{Nw}) = current\ coefficient\ w.r.t.\ \gamma_{rw}$$

$$\gamma_{rw} = relative\ wind\ direction$$

$$V_{rw} = relative\ wind\ velocity$$

Equation 23: Wind Forces

$$\boldsymbol{\tau}_{wind} = \frac{1}{2}\rho_w V_{rw}^2 \begin{bmatrix} C_{Xw}(\gamma_{rw})A_{Fw} \\ C_{Yw}(\gamma_{rw})A_{Lw} \\ C_{Nw}(\gamma_{rw})A_{Lw}L_{oa} \end{bmatrix}$$

Equation 24: Wind Force Matrix

$$\gamma_{rw} = \psi - \beta_w - \pi$$

Where:

$$\gamma_{rw} = wind\ relative\ angle\ of\ attack$$

$$\psi = vessel\ heading$$

$$\beta_w = wind\ inertial\ frame\ direction$$

Equation 25: Relative Wind Calculation

In order to calculate the frontal and lateral cross-sectional areas of the vessel an approximation was done by using a grid and utilizing images of the vessel (Figure 7). When it came to generating the wind signal the Simulink block acquired from the Marine Systems Simulator (MSS) was utilized as in the wave simulation [4]. This block generates wind speed and direction based on the mean angle and mean wind speed. The total velocity is composed of a slowly-varying mean superimposed with gusts based on a chosen wind spectrum. The direction is slowly-varying based on a random process [4]. Figure 8 shows an example of the wind environmental forces applied to the simulation model.
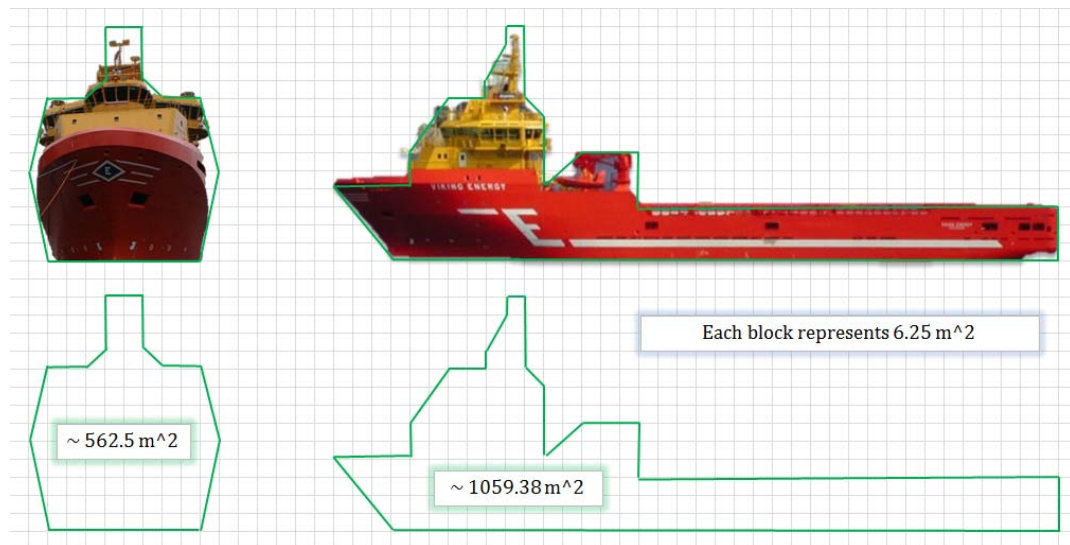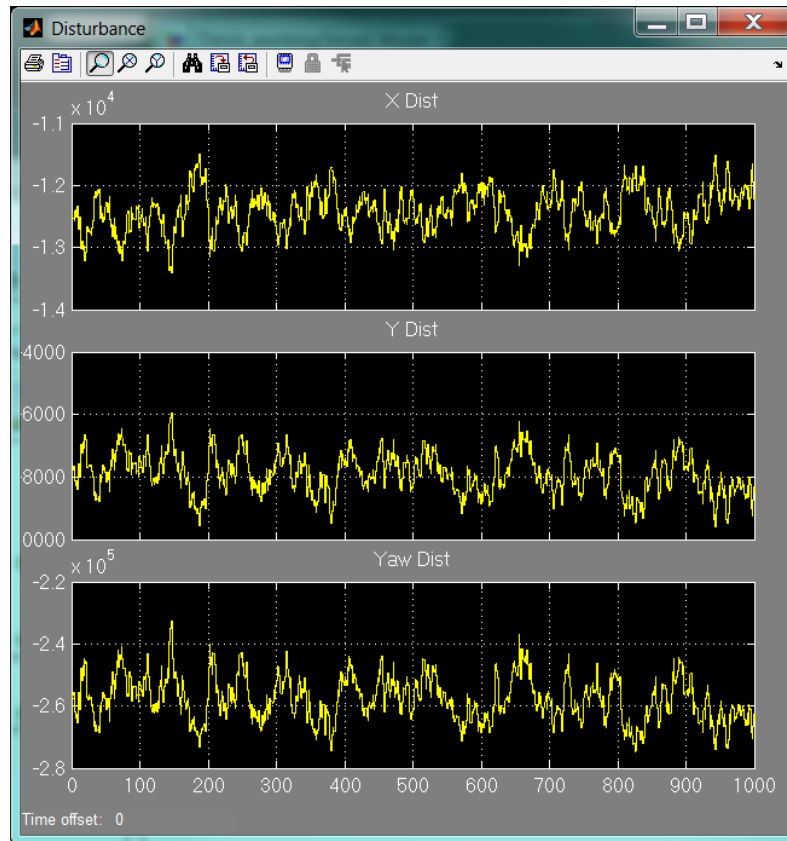

Figure 7: Wind Cross-Sectional Area

Figure 8: Wind Disturbance Forces and Moment

2.2.4.   Sensor Noise

Sensor noise is a common occurrence in any system and since this project was conducted on a simulation platform these noise disturbances needed to be created. The noise put onto the system was based on the Airmar PB200 WeatherStation® which measures both GPS location and heading. This weather station has an accuracy of within 2° on the heading and within 3 meters from the GPS [15]. The GPS accuracy is dependent on the number of satellites the weather station has access to but the values from the Airmar PB200 specifications document were determined to be adequate for this exercise. The noise added was a high frequency signal since most sensor noise signals are of this form. Figure 9 shows and example of the signals used to disturb the position data.
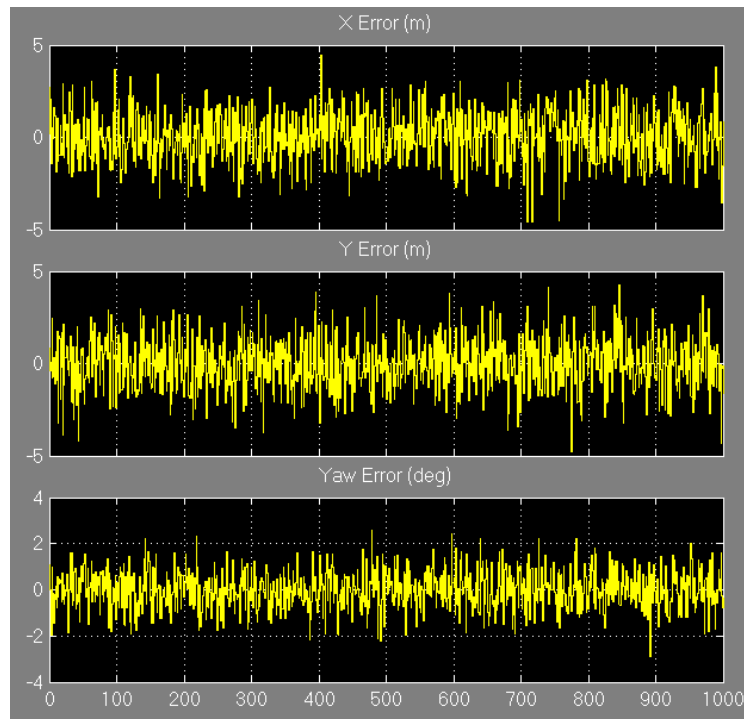
Figure 9: Sensor Noise

2.3. Actuators

The actuators for this system are the two azimuthal thrusters introduced earlier. These two thrusters are the same size and therefore produce the same thrust levels however they are located at different distances from CG, resulting in different torque arms. It will be shown later in the control section that since CG is not located at the central point between these two thrusters, the sway and rotation are coupled while the surge is decoupled from the other two. Both thrusters are controlled by sending a polar representation of the desired thrust level (u_i) and a rotational direction (α_i). Using these inputs, the simulation model decomposes the commands into the Cartesian equivalent values (u_{xi}, u_{yi}). The simulation creates the actuator forces on the vessel model based on the azimuthal thruster locations relative to CG and the

maximum thrust capabilities. Calculation of these thrusters' forces are shown in Equation 26 and Equation 27. Figure 10 illustrates the implementation on the vessel along with force vectors. It should be noted that since each thruster is referenced from CG, the aft thruster length (l_{x1}) is negative due to its negative location in the X axis from CG.

$$X = K_1 u_{x1} + K_2 u_{x2}$$

$$Y = K_1 u_{y1} + K_2 u_{y2}$$

$$N = l_{x1} K_1 u_{y1} + l_{x2} K_2 u_{y2}$$

Where:

$$K_i = Thruster\ max\ value$$

$$l_{xi} = Thruster\ X\ position\ relative\ to\ CG$$

$$u_{xi}\ and\ u_{yi} = X, Y\ thrust\ components$$

Equation 26: Azimuthal Thruster Forces

$$\boldsymbol{u}_a = \begin{bmatrix} u_{x1} \\ u_{y1} \\ u_{x2} \\ u_{y2} \end{bmatrix}$$

$$\boldsymbol{K}_a = diag(K_1, K_1, K_2, K_2)$$

$$\boldsymbol{T}_a = \begin{bmatrix} 1 & 0 & 1 & 0 \\ 0 & 1 & 0 & 1 \\ 0 & l_{x1} & 0 & l_{x2} \end{bmatrix}$$

$$\boldsymbol{\tau}_a = \boldsymbol{T}_a \boldsymbol{K}_a \boldsymbol{u}_a$$

Equation 27: Matrix Form of Azimuthal Thruster Forces
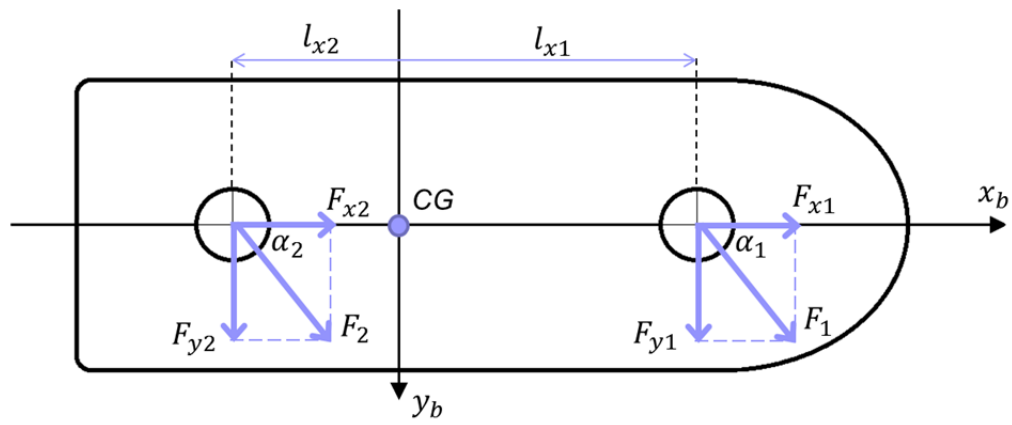
Figure 10: Azimuthal Thruster Diagram

Chapter 3

Controller Design and Evaluation

3.1. Introduction

There were several parts involved in the design of the controller for this DP simulation. For this system a Linear Quadratic Gaussian (LQG) controller was selected which regulates a linear system perturbed by white (Gaussian) noise by minimizing a quadratic control cost function. The LQG is comprised of a Linear Quadratic Regulator (LQR) and a Linear Quadratic Estimator (LQE). The LQE is often referred to as an observer or Kalman Filter. In an LQG implementation it is common for some of the states to not be measured but rather estimated. LQG controllers can be used in Linear Time-Invariant (LTI) and Linear Time-Varying (LTV) systems however, this system is LTI since the output does not depend on the time of the input. Stated simply, if an input is applied to a LTI system at some time the output would be the same as if applied at some Δt. Some considerations must be taken into account when using an LQG controller. One such concern is that the noise on the system must be Gaussian white noise. The other concern is that since this controller is of a linear basis, the system needs to be linearized around some point.

3.2. Linear System Model

3.2.1. Linearized System Model

Since this design is for a DP system which emphasizes zero movement the most logical point around which to linearize is zero velocity. When looking at the damping of the system the linear components dominate over the quadratic as seen in Figure 11. Below demonstrates how the original system model equations of motion (Equation 20) were linearized with the strike through terms equating to zero. The resulting linearized equation used for the LQG is shown in Equation 28.

$$M\dot{v} + C(v)v + Dv + d(v)v = \tau$$

$$\dot{v} = M^{-1}(\tau - C(v)v - Dv - d(v)v)$$

Using Taylor Series Expansion:

$$f(v) = \dot{v}, \quad v_0 = 0$$

$$f(v_0 + \Delta t) = f(v_0) + f'(v_0)\Delta t + H.O.T.$$

$$f(v_0) = M^{-1}\tau$$

$$f'(v_0) = -M^{-1}D$$

$$\dot{v} = M^{-1}\tau - M^{-1}Dv$$
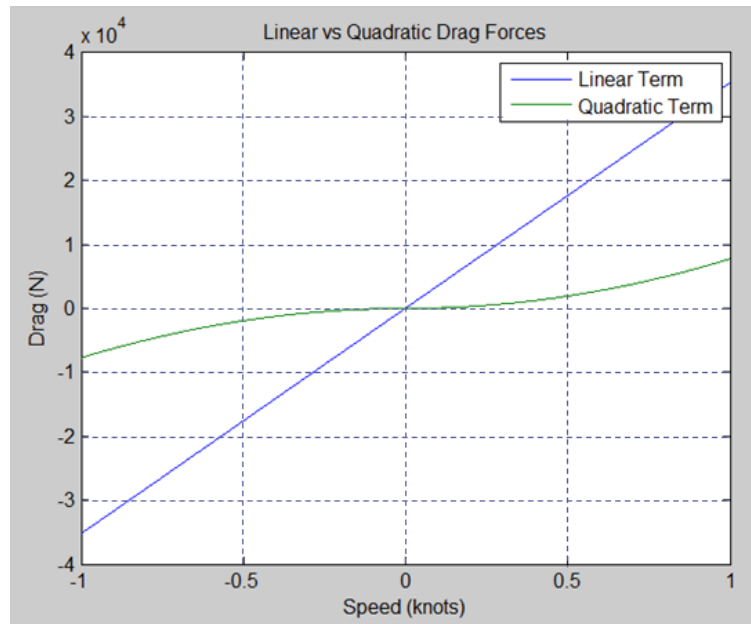
Equation 28: Linearized Vessel Model

Figure 11: Linear vs Quadratic Drag

With this definition of the linear system, it is apparent that the given plant (simulation model of the vessel) requires force/moment ($\boldsymbol{\tau}$) input, is dependant on velocity ($\boldsymbol{v}$) data, and outputs position ($\boldsymbol{\eta}$) information. The state space representation of this linear system can be expressed as shown in Equation 29.

$$\dot{\eta} = v$$

$$\dot{v} = -M^{-1}Dv + M^{-1}\tau$$

Therefore:

$$\dot{x} = Ax + B_u u$$

$$y = C_y x + D_u u$$

Where:

$$x = \begin{bmatrix} \eta \\ v \end{bmatrix}, \quad u = \tau, \quad y = \eta$$

$$A = \begin{bmatrix} 0 & I \\ 0 & -M^{-1}D \end{bmatrix}$$

$$B_u = \begin{bmatrix} 0 \\ M^{-1} \end{bmatrix}$$

$$C_y = \begin{bmatrix} I & 0 \end{bmatrix}$$

$$D_u = \begin{bmatrix} 0 \end{bmatrix}$$

Equation 29: Plant State Space Model

Before proceeding any further, it is important to determine if the plant is observable and controllable. This was accomplished by verifying the controllability and observability matrices were full rank. For this state space implantation full rank would equate to a value of six which has been illustrated in the figure and therefore the system is both controllable and observable. It is also important to note that the state space model shown in Equation 29 is one that does not incorporate noise or input and output gains. For a more complete model of the plant state space, one must include the state disturbances (environmental) and output disturbances (sensor noise). It is also useful to define gains for the states (x) and inputs (u) such that one is able to better regulate the control system. By adding these gains someone can limit over actuation and even prioritize the regulation terms. These terms are added as another output to the system (z) and are taken into account when calculating the LQR gain. The complete plant state space model is shown in Equation 30 and illustrated in Figure 12.

$$\dot{x} = Ax + B_u u + B_w w$$

$$y = C_y x + D_v v_n$$

$$z = C_z x + D_{zu} u$$

Where:

$$w = state\ noise$$

$$v_n = output\ noise$$

$$B_w = state\ noise\ gain$$

$$D_v = output\ noise\ gain$$

$$C_z = state\ gain$$

$$D_{zu} = input\ gain$$

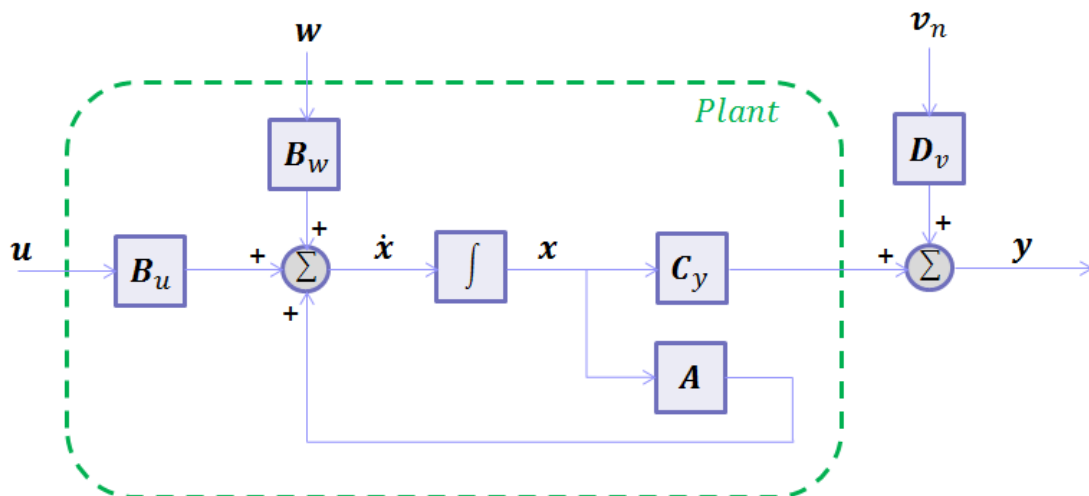Equation 30: Full Plant State Space Model

Figure 12: Plant Block Diagram

3.2.2.   Observer Based Controller

In an observer based implementation the observer attempts to estimate the unmeasured internal states of the plant as well as the expected outputs of the plant. The controller then uses that data to determine control signals to regulate the system. These estimated states are accomplished by knowledge of the system model of the plant. As mentioned before, not all states in the system can or will be measured. Using the state space model from Equation 30, it is possible to estimate the unmeasured components of the state.

When looking at the LQR component of the LQG controller, the objective is to compute a state feedback controller gain (K) which stabilizes the closed loop system and minimizes the objective cost function (Equation 31). The LQE components objective is to compute the observer gain (F) such that it stabilizes the state estimation error and minimizes the cost function shown in Equation 32.

$$J := \int_0^\infty x^T Q x + u^T R u \, dt$$

Where:

$$Q = C_z' C_z$$

$$R = D_{zu}' D_{zu}$$

Equation 31: LQR Objective Function

$$J := \int_0^\infty w^T Q_n w + v_n^T R_n v_n \, dt$$

Where:

$$Q_n = B_w B_w'$$

$$R_n = D_v D_v'$$

Equation 32: LQE Objective Function

Given the LTI system shown in Equation 30 we are able to compute the regulator gain (K) and the estimator gain (F) to be applied to the state space model of the observer based controller (Equation 33). When substituting for the input and the estimated output, we are able to get the closed loop LQG state space which is shown in Equation 34. This LQE controller block diagram is shown in Figure 13.

$$\widehat{x} = A\widehat{x} + B_u u + F(\widehat{y} - y)$$

$$\widehat{y} = C_y \widehat{x}$$

$$u = K\widehat{x}$$

Where:

$$K = -lqr(A, B, Q, R)$$

$$F = -lqr(A', C', Q_n, R_n)$$

Equation 33: Observer State Space Model

$$\widehat{x} = \left(A + B_u K + FC_y\right)\widehat{x} - Fy$$

$$u = K\widehat{x}$$

Equation 34: Closed Loop Observer

Figure 13: Controller Block Diagram

Now that we have both the vessel state space model and the closed loop controller we can check the stability of each of them by looking at their eigenvalues. Since the vessel model is a highly damped system it is expected that the plant would have stable eigenvalues. To verify everything was put together correctly, the eigenvalues are shown in Table 1. Also included in the table are the closed loop gains for the regulator and estimator with all the gains (Q, R, Q_n, R_n) set to identity matrices prior to doing any tuning. Since all the eigenvalues are in the left hand plane (LHP) the closed loop controller is stable. As one may also notice, their eigenvalues are exactly the same as a result of the plant already being stable. Since there are no disturbances to account for, the best controller is one which does nothing. Again, this controller is being optimized to hold position and if there is not a disturbance to push it off of position, there is no need to run the actuators. To further illustrate that the controller is virtually none responsive, Figure 14 shows how the linear system responds to the vessel

starting at an offset position. The figure demonstrates that the control forces created by the control loop are essentially zero and that the vessel makes no attempt to correct its position.

Table 1: Untuned Plant and LQG Eigenvalues

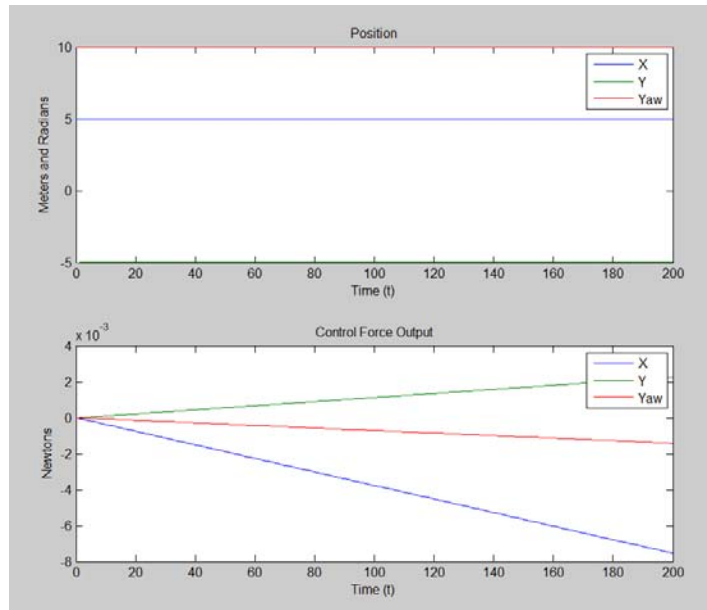| Plant	K	F
0	0	0
0	-0.0389	-0.0389
-0.1172	-0.0949	-0.1172
-0.0949	-0.1172	-0.0949
0	0	0
-0.0389	0	0

Figure 14: Untuned Closed Loop Response to Offset

The next step in the process was to minimize the cost functions for an expected disturbance. Since this is a simulation it is reasonable to have knowledge of the level of disturbance forces applied to the system and therefore set up the controller accordingly. For this simulation, the maximum expected value of the disturbances was on the order of 10^5, which equates to a 4 meter (~13 foot) wave height. Therefore the magnitude of $\boldsymbol{B}_w$ was set to

a magnitude of 10^5. By adding this to the control loop, it relays to the controller that there may be a large amount of external forces that will need to be overcome to function properly. To validate the control loop prior to attempting on the non-linear model, the linear model was used for the initial tuning resulting in favorable vessel response as shown in Figure 15. From the figure it is apparent that this control loop is capable of maneuvering the vessel back to the zero position. In this simulation there are no environmental disturbances or sensor noise and this is controlling the linear system it was specifically designed for. The next step in the evolution is to evaluate how this control operates on the non-linear model of the vessel.
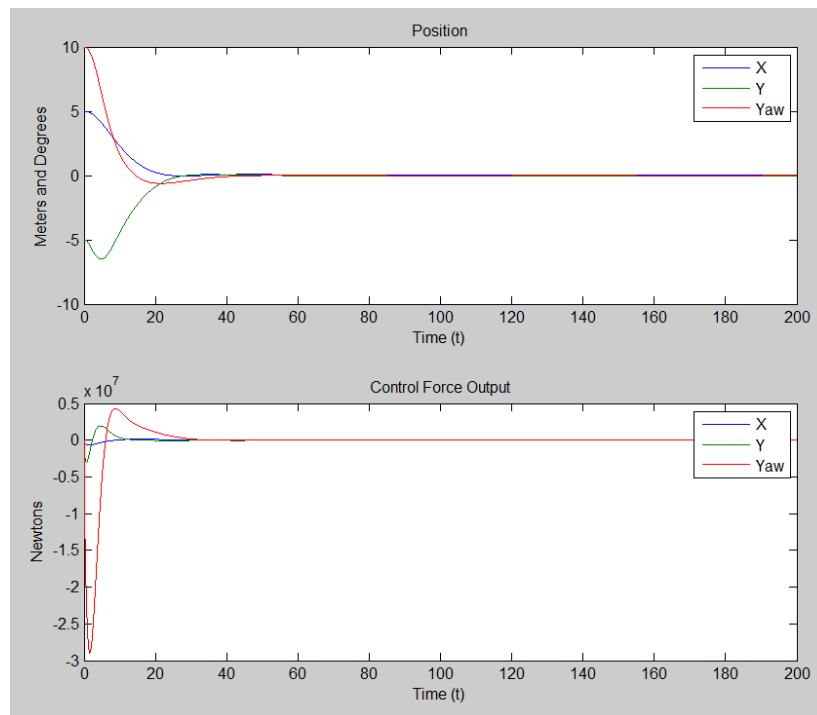

Figure 15: Tuned Control Loop of Linear Model

3.3. Non-Linear System Model

The first test of the LQG controller was to perform the same test performed on the linear model (Figure 15). The test involved placing the vessel at an offset position and observing the response of the closed loop system. The non-linear closed loop system performed relatively well without any disturbances (Figure 16). The control did overshoot the target point before stabilizing on all three axes but the (x, y) overrun remained below 5 meters and the yaw error stayed below 5 degrees. With the satisfactory performance, the next test in the progression was to begin adding disturbances.
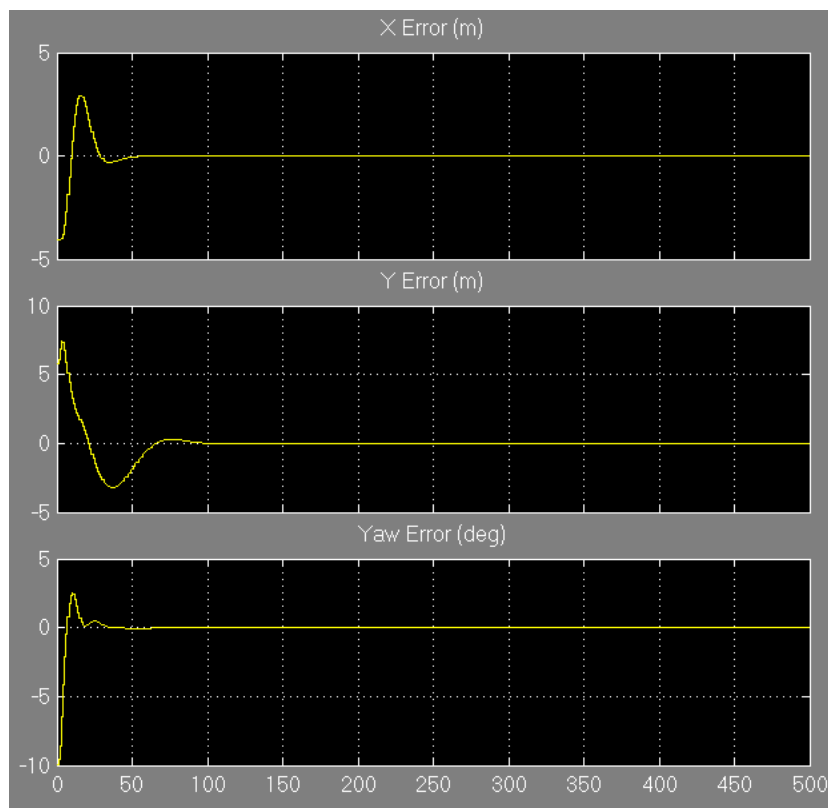

Figure 16: Non-linear w/o Disturbances

The first disturbance added was an ocean current. After some experimentation, it was determined that the worst case scenario was with a current applied at 45 degrees off broadside

of the vessel. This invoked the most force components for both X and Y as well as the largest Yaw moment. After applying the ocean current, the control loop was able to stabilize the vessel but it came to a stability point which was not the desired location (Figure 17). After some further tuning, which failed to resolve the issue, it became apparent that the controller would require an integral term to make up for this constant error value.
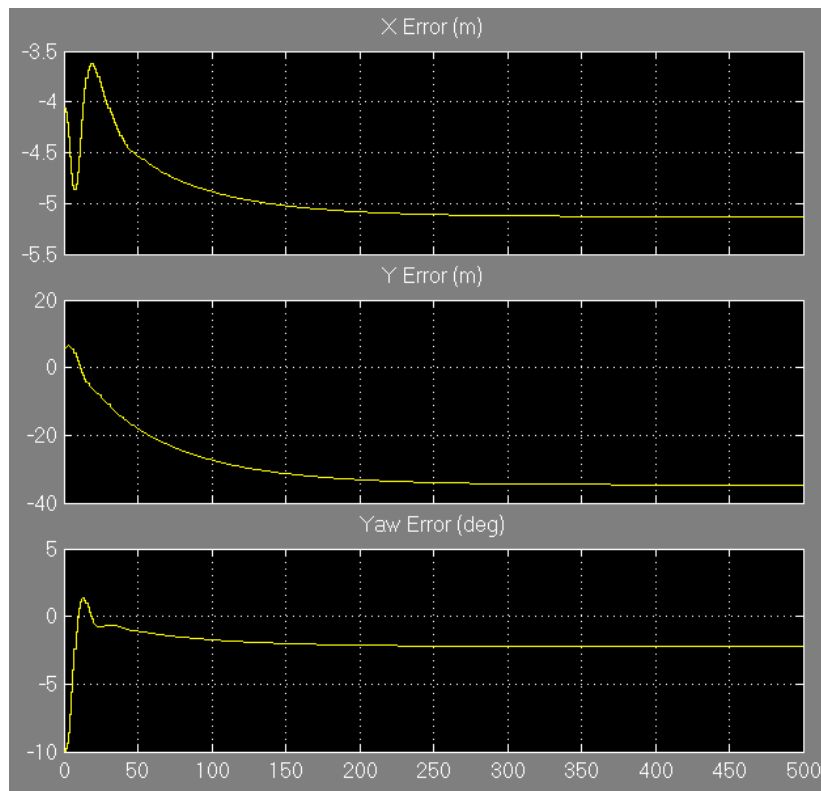

Figure 17: Current Disturbance w/o Integral Component

3.3.1.   Observer Based Controller With Integral Component

Adding an integral term to the control loop can be accomplished by adding another state to the state vector (Equation 35) which maintains the integrated error value within the LQG controller. This change in the state vector requires a change in the state space model to

account for the extra integral terms. This new state space is broken down into each matrix in Equation 36. One thing to note is that the Kalman filter (F) does not change in this implementation although the regulator gain (K) is altered and shown in Equation 37. The resulting LQG controller is the new observer based controller and is shown in Equation 38. The block diagram of the integral added LQG controller is shown in Figure 18 while the entire block diagram is displayed in Figure 19.

$$\tilde{x} = \begin{bmatrix} x \\ e \end{bmatrix}$$

Where:

$$e = \bar{y} - y, \qquad e = \bar{y} - C_y x$$

$$\bar{y} = desired\ position$$

Equation 35: Augmented State Vector

$$\dot{\tilde{x}} = \begin{bmatrix} A & 0 \\ -C_y & 0 \end{bmatrix} \tilde{x} + \begin{bmatrix} B_u \\ 0 \end{bmatrix} u$$

$$\tilde{z} = \begin{bmatrix} C_z & 0 \\ 0 & Q_i^{\frac{1}{2}} \end{bmatrix} \tilde{x} + \begin{bmatrix} D_{zu} \\ 0 \end{bmatrix} u$$

Where:

$$\tilde{A} = \begin{bmatrix} A & 0 \\ -C_y & 0 \end{bmatrix}$$

$$\tilde{B} = \begin{bmatrix} B_u \\ 0 \end{bmatrix}$$

$$\tilde{C} = \begin{bmatrix} C_z & 0 \\ 0 & Q_i^{\frac{1}{2}} \end{bmatrix}$$

$$\tilde{D} = \begin{bmatrix} D_{zu} \\ 0 \end{bmatrix}$$

$$Q_i = integral\ gain$$

Equation 36: Augmented State Space

$$K_i = -lqr(\widetilde{A}, \widetilde{B}, \widetilde{C}'\widetilde{C}, \widetilde{D}'\widetilde{D})$$

Where:

$$K_i = [K_x \quad K_e]$$

$$K_x = regulator\ gain$$

$$K_e = error\ gain$$

Equation 37: Regulator Gain with Error

$$\dot{\hat{x}} = A_c x + B_c u$$

$$u = C_c x$$

Where:

$$A_c = \begin{bmatrix} (A + B_u K_x + F C_y) & K_e \\ 0 & 0 \end{bmatrix}$$

$$B_c = \begin{bmatrix} F \\ I \end{bmatrix}$$

$$C_c = K_i$$

Equation 38: LQG with Integral

Figure 18: LQG Controller with Integral

Figure 19: Complete Control System

Performing the same ocean current test as with the non-integral LQG implementation results in significant improvements. Figure 20 demonstrates how the controller reacts to the current pushing it off the reference point. As evident in the plot, there is a delay in response which is most prevalent in the Y axis. This is due to the large compensation response from the controller attempting to maintain the yaw position. As discussed earlier, the Y and Yaw states are coupled where the X axis is uncoupled and free to react without interfering with the other two. With a vessel this large (~90 meters in length), the response appears to be

practical. Now that the control loop is successfully performing DP on a vessel in a current, the next step is to apply the other disturbances.
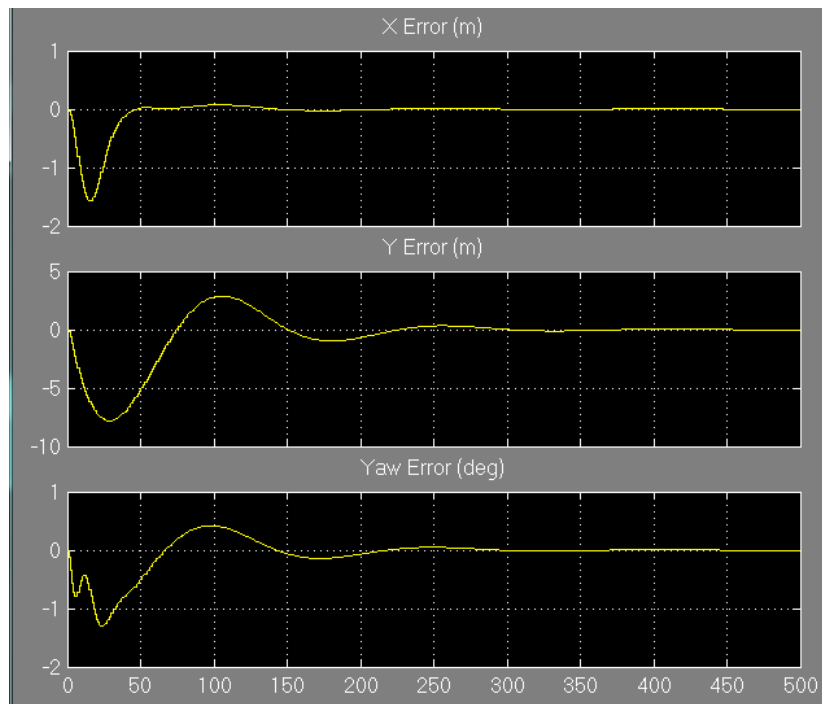

Figure 20: Current Applied to LQG with Integral

The LQG controller had no problem adding the rest of the environmental disturbances since they were properly accounted for in the early design phases. Figure 21 exhibits the behavior of the system when disturbed by a 2 knot current, 13 foot waves and a 60 knot wind. As described earlier in the environmental section a 2 knot current is rarely seen in ocean current velocities as most are below 1.5 knots. A 13 foot wave equates to very rough seas or otherwise referred to as a sea state 6 while the 60 knot wind is considered a storm wind speed [16]. Therefore this system is operating under reasonably extreme conditions. Another useful item to look at is the azimuthal thruster commands (Figure 22).
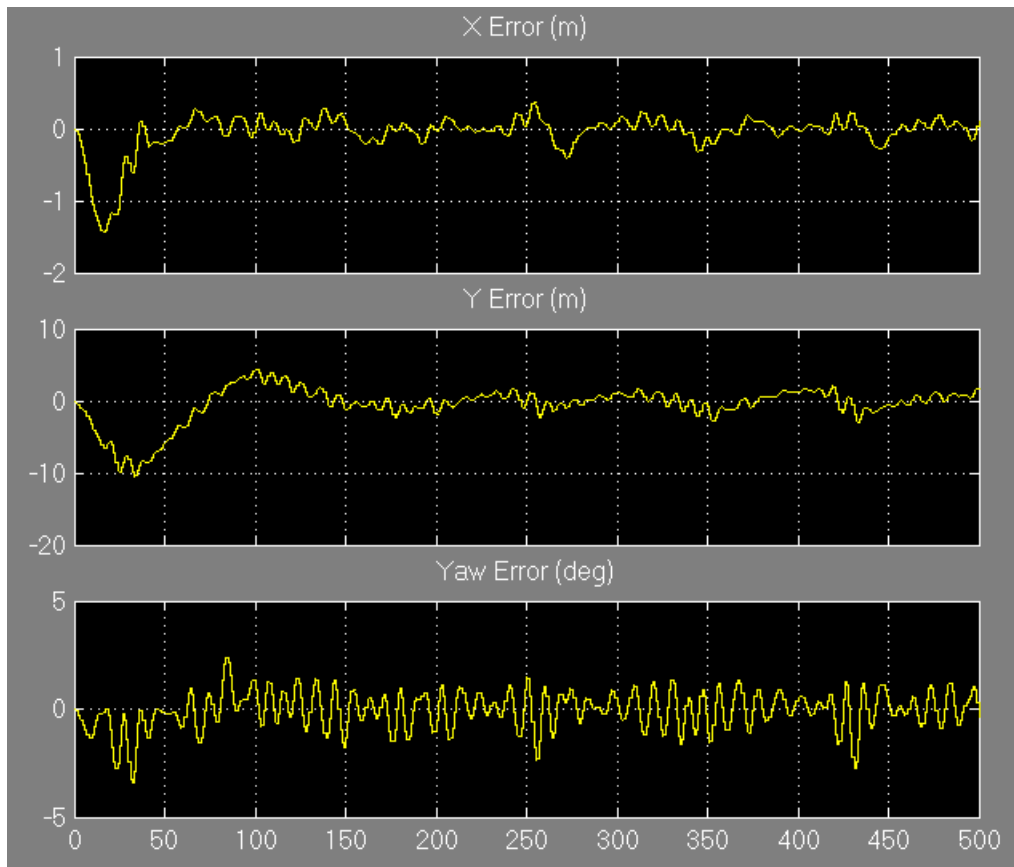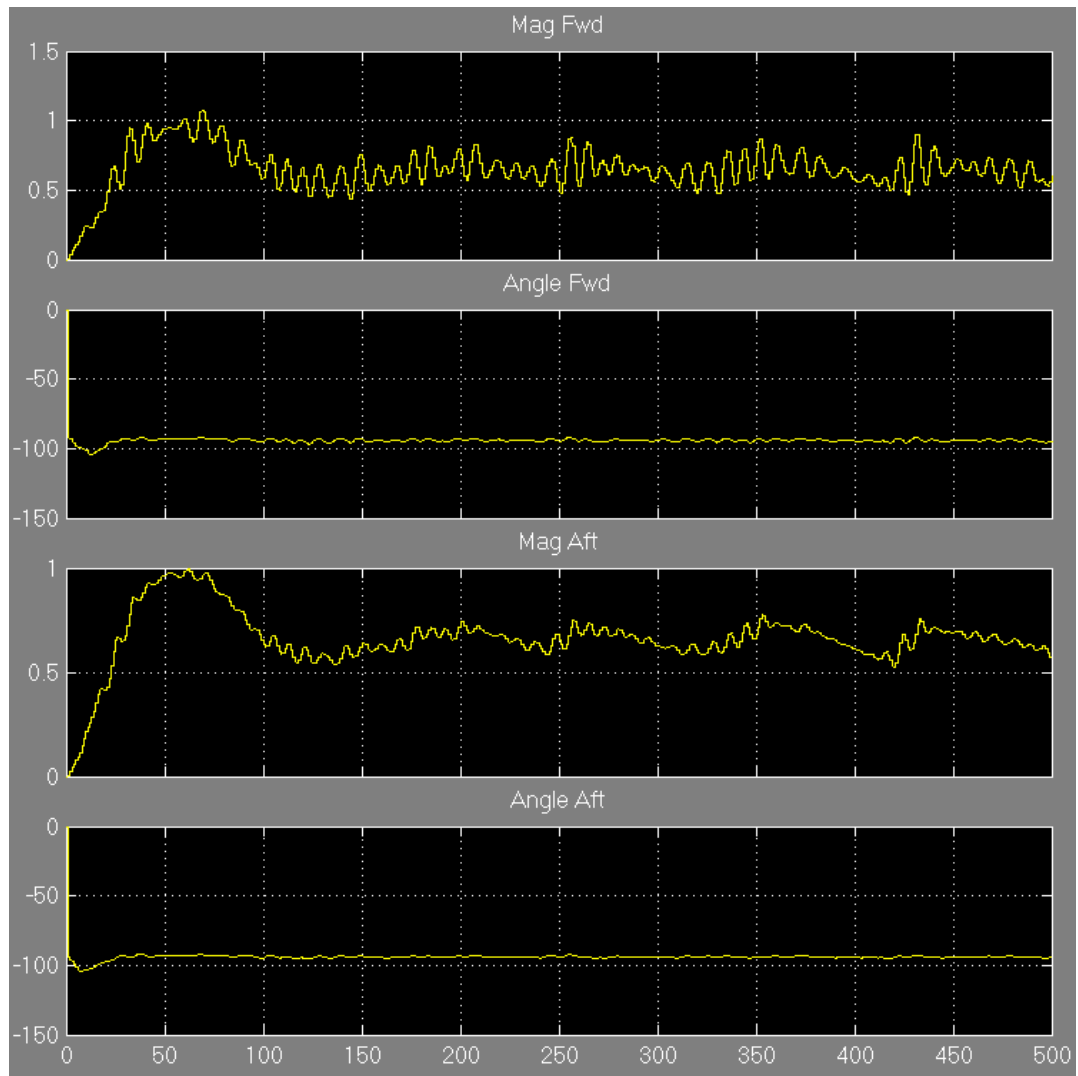
Figure 21: DP with Full Environment

Figure 22: Azimuthal Thruster Commands

The azimuthal thrusters are running near maximum to maintain the position during all the environmental disturbances. The thrust commands for this simulation range from 0-1 which equates to 0-100% of maximum thrust. The figure shows that the magnitudes for the forward and aft thrusters are nearly at maximum level while maintaining position.

The last piece to add to the simulation is the sensor noise. Upon adding this component, the controller continues to maintain the position effectively despite the inconsistency of the error data. Figure 23 shows both the error without the presence of noise

and the noisy error signal. This is effective to see how stable the overall system is operating with such a large noise variance. The variance in the error of the noisy signal adds a significant amount of variance to the signal even though, when looking at the actual vessel error, one can see that the vessel does not over actuate the system. The fact that the controller doesn't over actuate the system is better viewed on the azimuthal commands (Figure 24). It can be seen that the commands do not contain the same high frequency components as the sensor noise which could damage a mechanical system such as an azimuthal thruster.
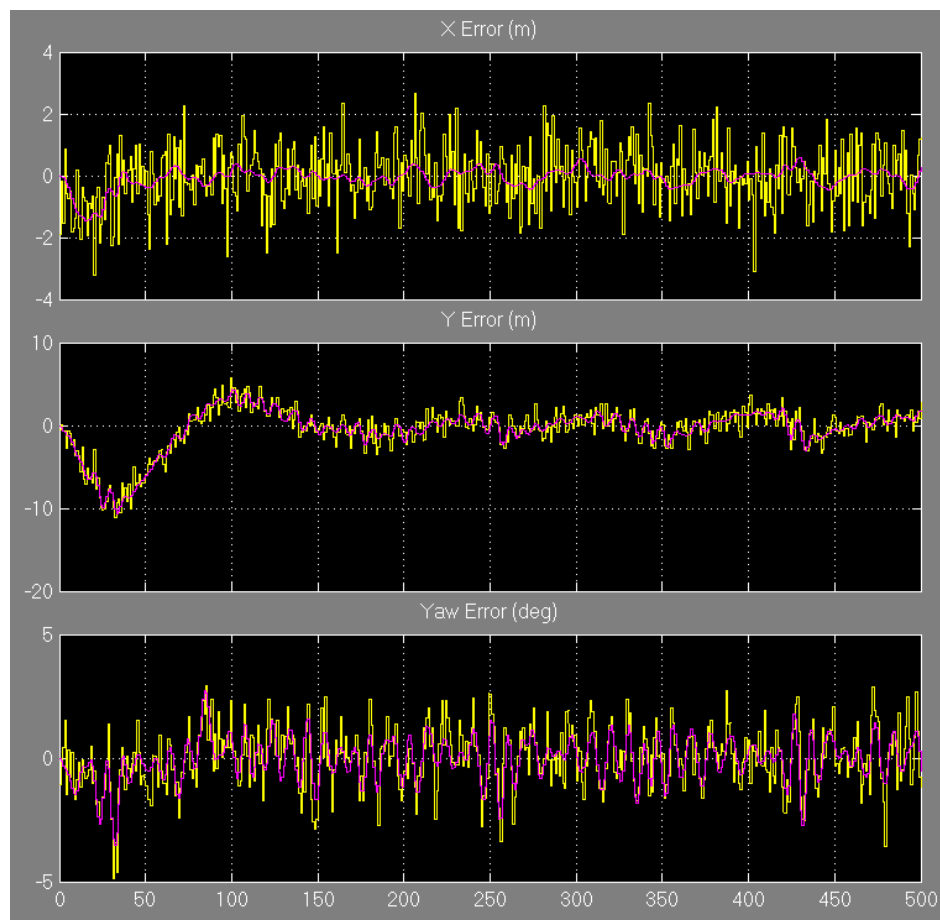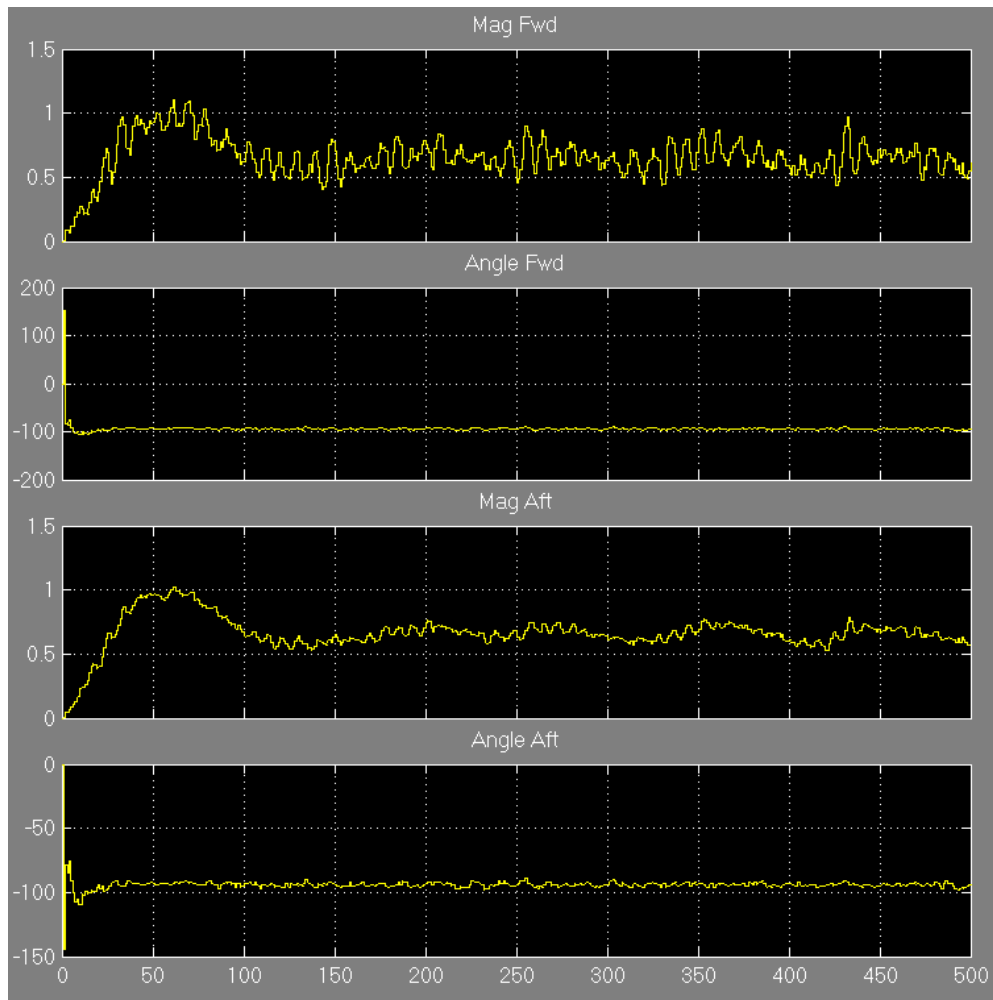

Figure 23: Error with Sensor Noise

Figure 24: Azimuthal Thruster Command for Sensor Noise

Given the harsh conditions of the environmental disturbances and the relatively large sensor noise added to the system this LQG process was a success. The system controlled the vessel by maintaining the desired position while not over actuating the thrusters. This control loop design, coupled with the work done to create the test environment to accommodate the LQG validation, has been a valuable endeavor for a non-mechanical individual such as myself.

Although this control task was a successful endeavor there are several areas of research which would have benefit from further evaluation if more time and financial

assistance were available. If more time had been available, implementing a feed-forward wind component to the controller would have proved to be a useful addition to the system. Another consideration for further development would be to construct a Proportional Integral Differential (PID) control loop approach and compare the performance with the LQG method. Given extra time would also allow for further improvement in the simulation model to better reflect the mechanical system. Simulations are never going to a perfect representation of their mechanical counterparts and should be understood as such which is why there is always room for enhancement. Lastly, if more funds were available it would have been particularly useful to perform testing on a real platform with actual environmental disturbances. For obvious financial reasons this would have been a difficult task to accomplish but the information attained from such an evolution would have been valuable for understanding the differences between a shipboard employment and its simulation counterpart.

References

1. Fossen, Thor I. (2011). Handbook of Marine Craft Hydrodynamics and Motion Control. pp. 391.

2. Sørensen, A.J. and J.P. Strand (1998). Positioning of Semi-submersible with Roll and Pitch Damping. In: Procedings of the IFAC Conference on Control Applications in Marine Systems (CAM'98). Fukuoka, Japan. pp. 67-73.

3. "Dynamic Positioning" (2010). Retrieved April 20th, 2013, from <http://en.wikipedia.org/wiki/Dynamic_positioning>

4. "Marine Systems Simulator (MSS)" (2010). Retrieved April 20th, 2013, from <http://www.marinecontrol.org>

5. "Viking Energy" Photo. shipspotting.com (2005). Retrieved April 21st, 2013, from <http://www.shipsandoil.com/shipinformation/eidesvik/eidesvik.htm>

6. Fossen, Thor I. (2011). Handbook of Marine Craft Hydrodynamics and Motion Control. pp. 121-122.

7. "Marine Hydrodynamics Lecture 13" Retrieved April 21st, 2013, from <http://web.mit.edu/2.20/www/lectures/Lecture-2012/lecture13-2012.pdf>

8. "Coriolis Effect" (2013). Retrieved April 28th, 2013, from <https://en.wikipedia.org/wiki/Coriolis_effect>

9. Fossen, Thor I. (2011). Handbook of Marine Craft Hydrodynamics and Motion Control. pp. 153.

10. "Current Tutorial" (2007).Retrieved May 5th, 2013, from <http://oceanservice.noaa.gov/education/tutorial_currents/lessons/currents_tutorial.pdf >

11. "Ocean Current" (2013). Retrieved May 5th, 2013, from <http://en.wikipedia.org/wiki/Ocean_current >

12. "Speed of Ocean Currents" (2002). Retrieved May 5th, 2013, from <http://hypertextbook.com/facts/2002/EugeneStatnikov.shtml>

13. Fossen, Thor I. (2011). Handbook of Marine Craft Hydrodynamics and Motion Control. pp. 189.

14. Fossen, Thor I. (2011). Handbook of Marine Craft Hydrodynamics and Motion Control. pp. 199.

15. "PB200" (2011). Retrieved May 5th, 2013, from <http://www.airmartechnology.com/uploads/brochures/PB200.pdf>

16. Fossen, Thor I. (2011). Handbook of Marine Craft Hydrodynamics and Motion Control. pp. 190-200.